Applied Surface Science 265 (2013) 78–87

Contents lists available at SciVerse ScienceDirect

Applied Surface Science

journal homepage: www.elsevier.com/locate/apsusc

Synthesis of platinum–polyaniline composite, its evaluation as a performance boosting interphase in the electrode assembly of proton exchange membrane fuel cell

R. Jayasree, K. Mohanraju, L. Cindrella *

Fuel Cell Laboratory, Department of Chemistry, National Institute of Technology, Tiruchirappalli 620015, India

ARTICLE INFO

Article history:
Received 17 April 2012
Received in revised form 7 October 2012
Accepted 19 October 2012
Available online 9 November 2012

Keywords:
Polyaniline
Platinum
Composite
Gas diffusion layer coating
Proton exchange membrane fuel cell
Performance characteristics

ABSTRACT

Platinum formed on polyaniline (PANi) is used as the interlayer between porous gas diffusion layer and the catalyst layer with the aim to reduce the thickness of the ordinary gas diffusion layer and provide a performance boosting electrostatic layer. The doping tendency of PANi is utilized to incorporate platinum(IV) ion in its matrix by chemisorption followed by its reduction to metallic platinum. Platinum is deposited on polyaniline by a simple wet chemistry method. PANi is prepared by the chemical oxidative polymerization of aniline by ammonium persulphate while Pt deposition on PANi is achieved by a phase transfer method (water–toluene) to yield Pt nanoparticles on PANi. The composite is characterized by XRD, Scanning electron microscopy (SEM) with energy dispersive X-ray analysis (EDX), IR spectroscopy, cyclic voltammetry (CV), AC impedance studies, density and conductivity measurements. The Pt/PANi composite is assessed in the proton exchange membrane fuel cell (PEMFC) using H_2/O_2 gases at ambient pressure. The performance of the PEMFC with Pt/PANi composite interphase on cathode side of the gas diffusion layer (GDL) shows improvement at high current densities which is attributed to the increased capacitative current of Pt/PANi layer in the presence of O_2 thereby improving the kinetics of subsequent reduction of O_2.

1. Introduction

Proton exchange membrane fuel cell (PEMFC) is considered to be the most attractive energy technology for the future due to its advantages such as increased efficiency, high power density, ultra low emissions of environmental pollutants, low weight, compact construction, and its ability to operate at lower temperatures (<100 °C) [1]. The PEMFC has undergone active developments over the recent years due to its very wide range of mobile applications, transportation applications and also in combined heat and power (CHP) systems. But commercially, the PEMFC still has a few hurdles to overcome such as reducing the material and catalyst costs, enhancing per weight use of platinum catalyst, and improving the performance of the membrane electrode assembly.

Efforts are going on for enhancing the performance of platinum catalyst in PEMFC. This may be done by increasing the surface area of the catalyst through homogeneous distribution on a high surface area support material or by miniaturization of the particle size of the catalyst at the nanoscale [2]. A wide variety of catalyst support materials having large surface area have been studied extensively for various applications. These include polymer nanocomposites [3], polyaniline (PANi) [4–6], multi-walled carbon nanotubes (MWCNTs) [7], single-walled carbon nanotubes (SWCNTs) [8], alumina (Al_2O_3) [9], nitrogen-doped magnetic carbon nanoparticles (N-MCNPs) [10], graphitized carbon nanofibres [11], nitrogen containing activated carbon fibre, polyamidoamine (PAMAM) dendrimers [12], etc. There has been a growing interest in research on conducting polymers because of the double advantages of being an organic conductor and highly conjugated polymeric structure, thus exhibiting attractive physicochemical properties for application in PEMFCs. The emeraldine salt form of polyaniline (PANi) [13], which is electrically conductive, can be synthesized in bulk and the cost of raw materials is very less. The unique properties of PANi are its good mechanical strength, tunable electronic and electrical conductivity, high chemical stability for use below 100 °C, large surface area, and simple and low cost manufacturing process. Platinum supported PANi prepared by various methods have been studied for their catalytic properties in redox reactions [14–17]. Composite of PANi and multiwalled carbon nanotube with immobilized Pt particles have been assessed for their redox characteristics [18].

With regard to the synthesis of platinum nanoparticles (Pt NPs), the literature reports various routes such as electrodeposition [19], sol–gel [20], micro-emulsion techniques [21], polyol process [22],

* Corresponding author. Tel.: +91 431 2503634; fax: +91 431 2500133.
E-mail address: cind@nitt.edu (L. Cindrella).

0169-4332/$ – see front matter © 2012 Elsevier B.V. All rights reserved.
http://dx.doi.org/10.1016/j.apsusc.2012.10.126

sonochemical synthesis [23], hydrothermal method [24], sputter deposition [25], pulsed laser deposition [26,27], radiation induced synthesis [28], solution reduction method [29] and chemical reduction of organometallic precursors and simple platinum salts [30,31]. Even though all these methods are efficient in producing a wide particle size range of Pt NPs, controlling the particle size continues to be the most difficult challenge because individual nanoparticles tend to agglomerate during the preparation process. Sputter deposition and pulsed laser deposition techniques though control particle size and agglomeration of the particles, their cost and non-suitability for large area deposition are their limiting factors. To overcome that, preparation of nanoparticles by simple chemical reduction of metal species at low temperatures and at room temperature has been reported for both aqueous and non-aqueous solutions. In addition, preparation of nano platinum by chemical reduction in viscous stabilizing medium has also been reported [32].

In the current work, the doping tendency of polyaniline (PANi) is exploited to incorporate platinum(IV) ion in its matrix by chemisorption followed by its reduction to metallic Platinum. PANi has the potential of a high area support material, on which platinum catalyst could be deposited. PANi was synthesized by the chemical oxidative polymerization of aniline and then platinum particles on PANi was prepared by first trapping the Pt(IV) ion onto PANi by ionic interaction, followed by chemical reduction of Pt(IV) ion to Pt^0 by sodium formate. The Pt/PANi nanocomposite was assessed in the proton exchange membrane (PEM) single cell using H_2/O_2 gases at ambient pressure. The fuel cell performance of MEA with Pt/PANi catalyst thin layer on GDL showed excellent improvement in the range of performance. The water balancing property of PANi provided the essential functionality for the support material. The Pt/PANi composite material was characterized by XRD, Scanning electron microscopy (SEM) with energy dispersive X-ray analysis (EDX), Infrared (IR) spectroscopy, cyclic voltammetry (CV) and AC impedance studies, density and conductivity measurements.

2. Experimental

2.1. Materials

All the chemicals used were AnalaR grade and double distilled water was used for the solution preparation. Hydrated hexachloroplatinic acid ($H_2PtCl_6{\cdot}6H_2O$), tetraoctyl ammonium bromide (TOAB, $N(C_8H_{17})_4Br$), toluene ($C_6H_5CH_3$), 1-dodecanethiol ($C_{12}H_{25}SH$, 98%), sodium formate (HCOONa), ammonium persulphate ($(NH_4)_4(SO_4)_2$), aniline, sodium sulphate, hydrochloric acid, sulphuric acid, acetone and absolute alcohol were used in the present study.

2.2. Synthesis of polyaniline

Polyaniline was synthesized by chemical oxidative polymerization of aniline in the presence of hydrochloric acid as a catalyst and ammonium persulphate as an oxidant by chemical oxidative polymerization method. In a typical synthesis, 25 mL of 0.2 M aniline solution was taken in a beaker and about 10 mL of 0.2 M hydrochloric acid was added to it. The beaker was kept in an ice bath maintaining a polymerization temperature of 0–5 °C. To this, 15 mL of 0.5 M ammonium persulphate ($(NH_4)_2S_2O_8$) maintained at around 5 °C was added slowly using a micro burette. The mixture was stirred continuously for an hour by an electromagnetic stirrer and the polymer precipitate was filtered in a G4 sintered crucible. The polymer was then washed with double distilled water till the filtrate became colourless. The precipitate was rinsed with 3 to 5 mL of acetone. The resultant PANi polymer was dried under vacuum at 60 °C overnight.

2.3. Deposition of platinum nanoparticles on polyaniline

About 0.1 M aqueous chloroplatinic acid ($H_2PtCl_6{\cdot}6H_2O$, orange coloured solution) was prepared in double distilled water and 0.2 M tetra-*n*-octyl ammonium bromide ($C_{32}H_{68}BrN$) (TOAB) solution was prepared using toluene as solvent. 3 mL of aqueous chloroplatinic acid was mixed with 4 mL of TOAB solution and was shaken for 30 min in a mechanical shaker at room temperature [33]. During this process, TOAB acted as the phase-transfer catalyst [34] by transferring $PtCl_6^{2-}$ ions from aqueous solution to toluene. The orange-coloured organic layer was separated, to which 2.5 g of PANi was added with constant stirring for 1 h. Thereafter, 0.65 mL of 1-dodecanethiol was added to act as the capping agent for the subsequently formed platinum particles and shaken for another 30 min. About 10 mL of 0.1 M aqueous sodium formate solution was added in drops to the above suspension and stirred continuously for another 2 h at 60 °C. The mixture was filtered through a G4 sintered crucible to remove solvent and the precipitate was thoroughly rinsed with copious amount of warm double distilled water to remove sodium formate and then with ethanol to remove the excess of 1-dodecanethiol. The scheme of preparation of Pt/PANi composite is shown in Fig. 1. The Pt/PANi product was dried overnight at 80 °C in vacuum oven and stored in dessicator. It contained 1.32% of platinum as revealed by EDX study. The density of PANi and Pt/PANi was measured by Helium Pycknometer (Pycno 30 True Density Meter, Smart Instruments Co. Pvt. Ltd., Thane, India) and the surface resistivity was measured by four probe device. Pellets of approximately 0.200 g weight were made for the studies of conductivity, cyclic voltammetry and impedance measurements.

2.4. Construction of membrane electrode assembly (MEA) and fuel cell evaluation

The gas diffusion layer (GDL) was prepared using Toray carbon paper. The carbon paper was first teflonised by 10 weight percentage of PTFE for hydrophobicity and the porous layer was provided by loading a slurry of Vulcan X (VX) Carbon and 30% PTFE, at a loading amount of 1 mg cm^{-2} of VX carbon by spraying method. The loading of 0.42 mg cm^{-2} of the Pt/PANi composite was coated on the GDL of cathode side. As PANi is a porous material, we have made the GDL without the macroporous layer (generally the GDL is prepared to consist of macro porous layer using carbon fibre in high content and a micro porous layer using VX carbon). The model of MEA prepared in this study is shown in Fig. 2.

Catalyst coatings were prepared on Nafion membrane (NRE 212) with 5 cm^2 active area by spraying catalyst ink prepared using commercial Pt/C containing 20% by weight of platinum, 5% nafion and isopropyl alcohol in nitrogen atmosphere, by the micro-spray method. The catalyst loadings on the anode and cathode catalyst layers of the reference MEA were about 0.30 and 0.50 mg Pt cm^{-2} respectively while the catalyst loadings on the anode and cathode catalyst layers of the MEA with Pt/PANi coated GDL were about 0.23 and 0.44 mg Pt cm^{-2}, respectively. The platinum loading on the reference MEA and the one prepared in this study are compared later with the data from the EDX study. The catalyst coated Nafion-212 membranes were vacuum dried at about 50 °C for 30 min before assembling in the single test cell.

The MEAs were fabricated by sandwiching the GDLs and the catalyst coated membrane inside the single cell test cell (Fuel Cell Technologies Inc., Albuquerque, NM, USA). Gas sealing was achieved using silicone coated fabric gasket and with a uniform torque of 0.45 kg m. The fuel cell performance was evaluated at 60, 70 and 80 °C at 100% RH conditions on both anode and cathode sides using Single Fuel cell Test Station (K-PAS Instronic Engineers India Pvt. Ltd., Chennai, India). The flow rates were fixed at 0.250 and 0.500 SLPM for H_2 and O_2, respectively. The steady state voltage

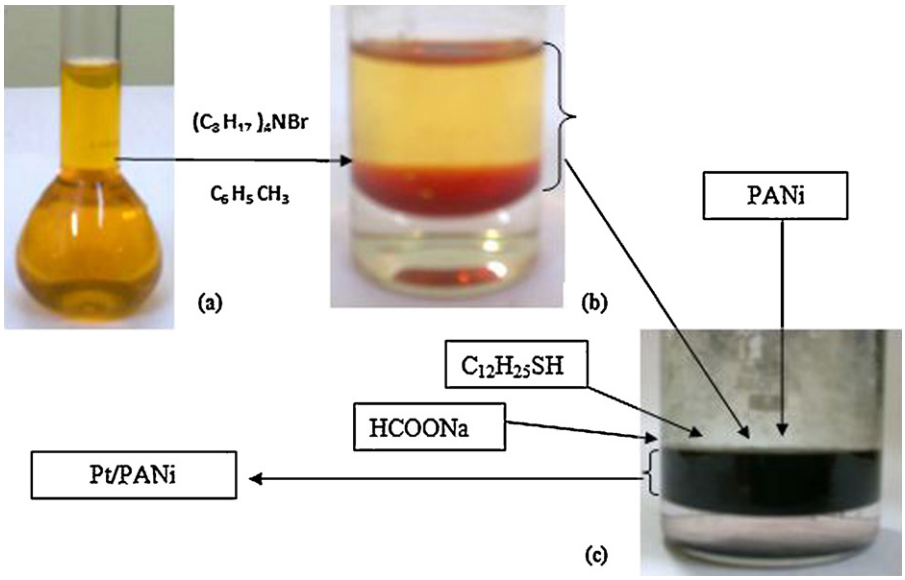

Fig. 1. Scheme of preparation of Pt/PANi composite: (a) hexachloroplatinic acid solution, (b) phase transferred Pt^{4+} ions, (c) reaction vessel showing the addition of (b), PANi, dodecane thiol and sodium formate, leading to the formation of Pt/PANi.

values were collected by holding the cell at each current density value for 30 s.

2.5. Characterization techniques

XRD study was carried out using Philips Powder diffractionmeter (Cu Kα radiation) to determine the crystallinity details of PANi and Pt/PANi along with the elemental information on Pt. The IR spectra of PANi and Pt/PANi were recorded to identify the structural changes on platinum loading. The surface topographies of PANi and Pt/PANi have been characterized by SEM using FEI Quanta 200 scanning electron microscope with energy dispersive X-rays (EDX) analysis. Cyclic voltammetry (CV) and AC impedance studies were also carried out using Electrochemical Work station (CH Instruments) to assess their electrochemical properties and to measure the charge transfer resistance of Pt/PANi in 0.1 M sulphuric acid and 0.1 M sodium sulphate solution in inert atmosphere as well as in oxygen atmosphere. The electrochemical study was carried out with silver-silver chloride electrode as the reference electrode, platinum as the counter electrode and the pelletized PANi and Pt/PANi as the working electrode. The electrical contact on the working electrode was provided with conducting silver paste. An area of 0.6132 cm^2 of the working electrode was immersed in the conducting medium for the electrochemical study. CV was studied at a scan rate of 20 mV s^{-1}. The AC impedance study was carried out in the frequency range of 1–100,000 Hz. The applied voltage for the impedance study was maintained at the open circuit voltage of the working electrodes (0.32 V for PANi and 0.44 V for Pt/PANi Vs Ag/AgCl).

3. Results and discussion

The UV–vis spectra of hexachloroplatinic acid in aqueous medium and in toluene are shown in Fig. 3. The spectra show quantitative transfer of Pt(IV) ion to the toluene layer. The phase transferred Pt(IV) ion shows interaction with TOAB as evident from the shift in the λ_{max} value to 316 nm from 310 nm for the aqueous

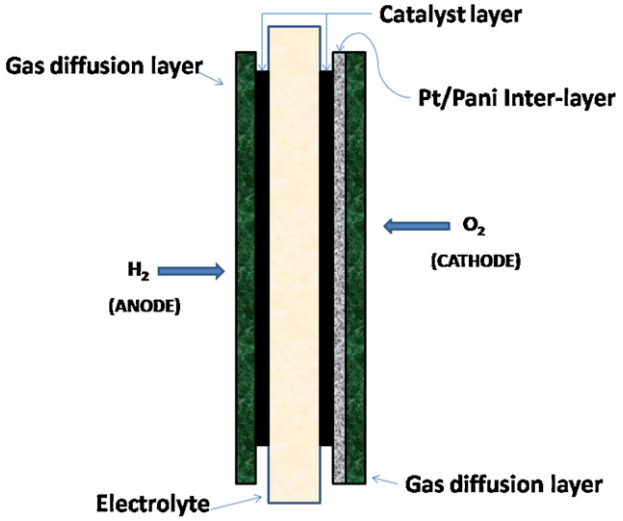

Fig. 2. Schematic representation of membrane electrode assembly in the presence of interphase.

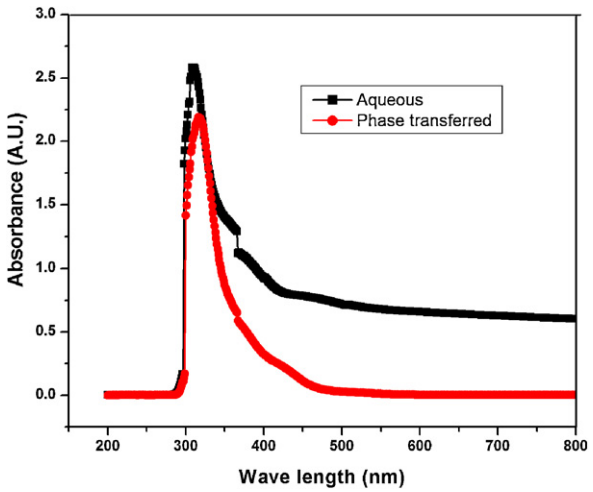

Fig. 3. UV–vis spectra of Pt^{4+} in aqueous medium and after phase transferred to organic layer.

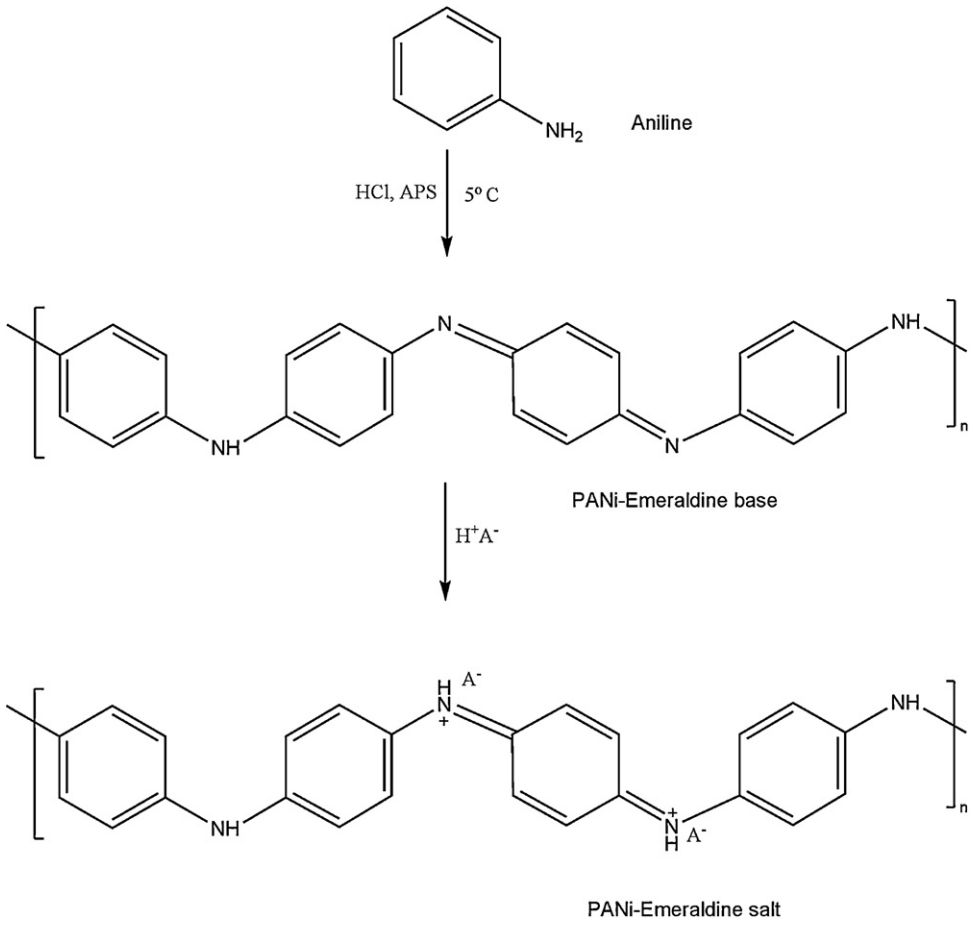

Fig. 4. Reaction scheme for aniline polymerization and doping with the formation of semi conducting emeraldine base and conducting emeraldine salt forms.

hexachloroplatinic acid solution. As the curve of the phase transferred ion did not show any additional peak at 310 nm, it confirmed the complete transfer to the organic layer and absence of any trace of water–toluene interface. This is in support to the observation of clear solution as the lower layer in Fig. 1b.

Formation of PANi from aniline and doping of one of its form (emeraldine base) with acid is shown in the reaction scheme (Fig. 4). When cation like Pt(IV) is added to the emeraldine base form of PANi, it shows ionic interaction with the cation. Subsequent reduction of Pt(IV) to Pt by the reducing agent allows the dispersion of Pt on PANi matrix. This principle has been used in this study to prepare Pt/PANi composite.

The X-ray diffraction patterns for PANi and Pt/PANi are given in Fig. 5. The XRD pattern of PANi (Fig. 5a) exhibits a semi crystalline structure. It shows a broad peak at $2\theta = 25.5^\circ$ corresponding to the (1 1 0) lattice plane [35–37]. The broad peak between $2\theta = 22^\circ$ and 28° is the characteristic of PANi [38]. The Pt/PANi composite (Fig. 5b) shows characteristic sharp peaks at $2\theta = 39.83^\circ$, 46.29° and 67.62° corresponding to the (1 1 1), (2 0 0) and (2 2 0) lattice planes [39] respectively of Pt (JCPDS file no. 04-0802), confirming the presence of Pt in the face-centred cubic (FCC) structure. While platinum retains its lattice form when dispersed in PANi matrix, there is change in the semi crystallinity of PANi. It is reasonable to believe that the small peaks at 31.78° and 33.77° are due to the changes in the crystalline structure of PANi due to the presence of Pt as they do not match with the characteristic indices of platinum and the peaks fall in the amorphous range of PANi (Fig. 5a). The average size of the PANi and Pt in Pt/PANi composite has been determined by the Debye–Scherrer equation after curve fittings and background subtractions.

According to Debye–Scherrer method, the approximate crystallite size of powder sample (d) can be determined by the following equation:

$$d = \frac{0.9\lambda}{\beta \cos \theta}$$

where λ is the wavelength of the X-ray radiation (0.154056 nm for Cu Kα), β is the full width at half maximum (FWHM) of the diffraction peak measured at 2θ (in radians), and θ is the Bragg's diffraction angle in degrees.

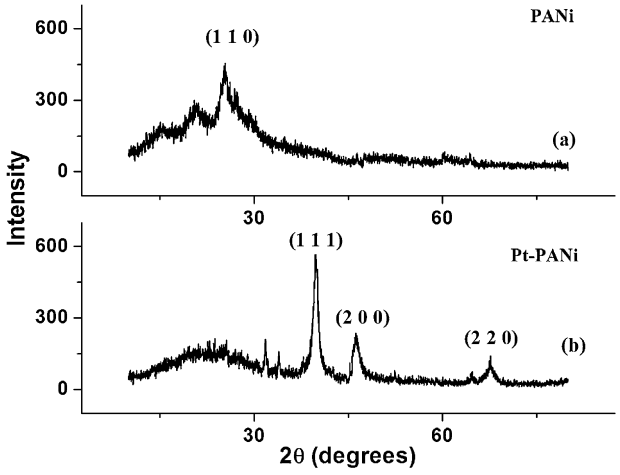

Fig. 5. XRD patterns of (a) PANi and (b) Pt–PANi composite.

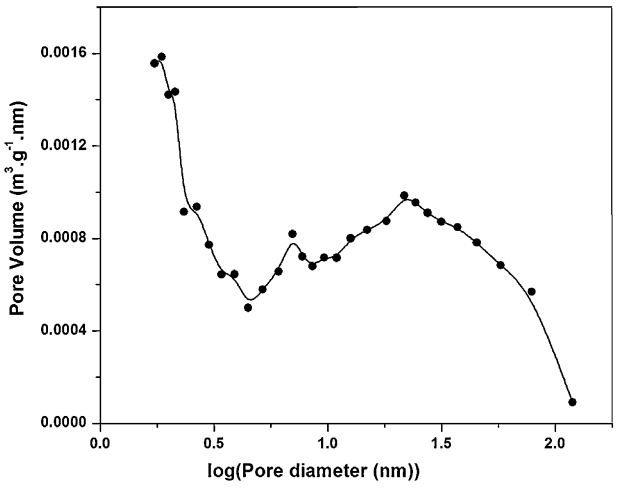

Fig. 6. Distribution of pore volume of Pt/PANi composite as the function of pore diameter.

The average crystallite size of PANi has been found to be approximately 4.01 nm. The average size of Pt in Pt/PANi composite has been found to be approximately 7.76 nm with the crystallite sizes ranging between 9.54 nm and 6.00 nm at the three different lattice planes. This confirms the nano scale of the Pt/PANi composite. The density of PANi was found to be 1.4894 g cm^{-3} while that of Pt/PANi composite was measured to be 1.8480 g cm^{-3}. Inclusion of platinum has resulted in the increase of density of the sample as expected.

BET surface area of the sample is 17 m^2 g^{-1}. The adsorption average pore diameter is 27 nm. The distribution of pore volume as a function of pore size is given in Fig. 6. Large fraction of the pore volume is by microporous (<50 nm) pores of the composite and majority of the pores have diameter less than 100 nm. Gradation in the pore volume also promises the continuous flow of the reactant gases without any pressure build up. PANi matrix also contained large open pores in macro porous range which generally cannot be accounted for by BET study.

Fig. 7 shows the SEM images of PANi (a and b) and Pt/PANi (c and d) each at 500 nm and 3 μm scales. Continuous matrix is evident from the 500 nm scale (Fig. 7a and c) and the large surface area and highly porous structure of the polymer material is observed from the 3 μm scale images (Fig. 7b and d). The presence of dispersed Pt particles could be better viewed in the back scattered SEM image (Fig. 7d). While the Pt particles in the PANi matrix are dispersed, they show agglomeration at some regions.

The transmission electron micrograph of the Pt/PANi is shown in Fig. 8a and b. Platinum particles within nano scale are observed from Fig. 8a, while the agglomeration could be observed in Fig. 8b. The drifting of PANi under TEM study made it difficult to focus the individual particles of Pt.

EDX spectra of PANi (Fig. 9a) and Pt/PANi (Fig. 9b) also confirmed the presence of Pt in PANi. The weight percentages of the elements in the samples are given as tables in the plots. While the PANi structure is constituted by carbon (C), nitrogen (N) and hydrogen (H), the peaks corresponding to C and N are as expected. EDX is not sensitive to the lighter atom H. But the

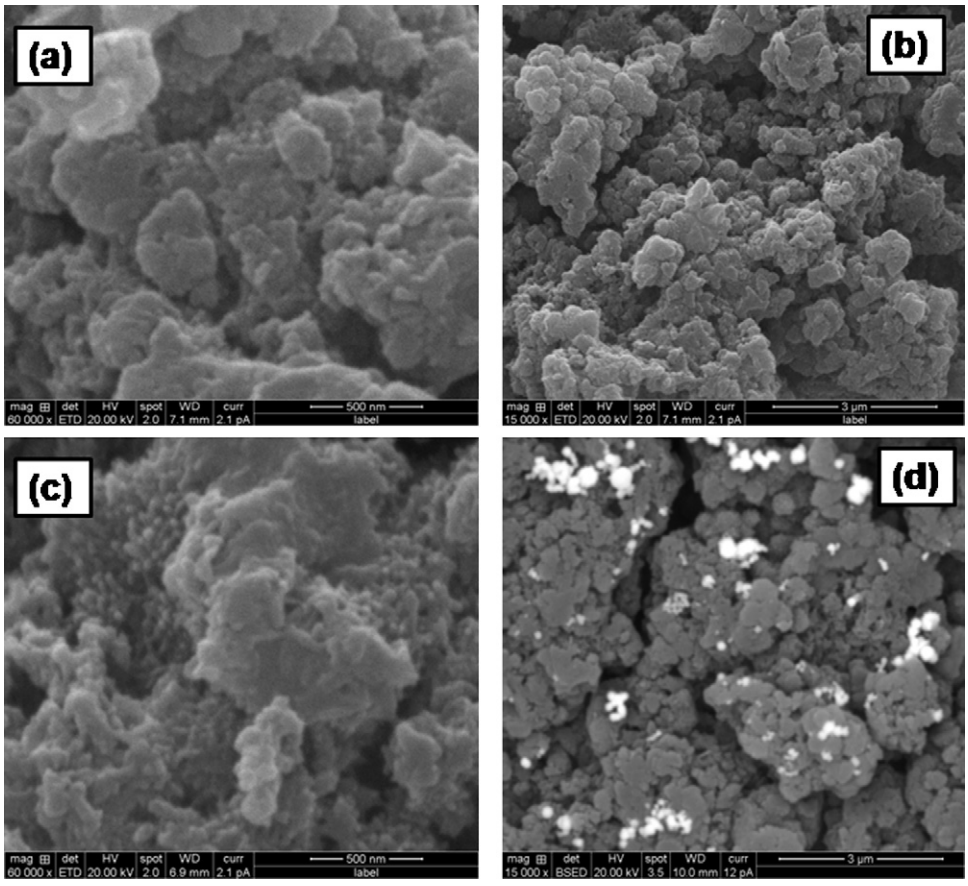

Fig. 7. SEM images of (a) PANi at 500 nm scale, (b) PANi at 3 μm scale, (c) Pt/PANi at 500 nm scale, and (d) Pt/PANi (Back scattered image) at 3 μm scale.

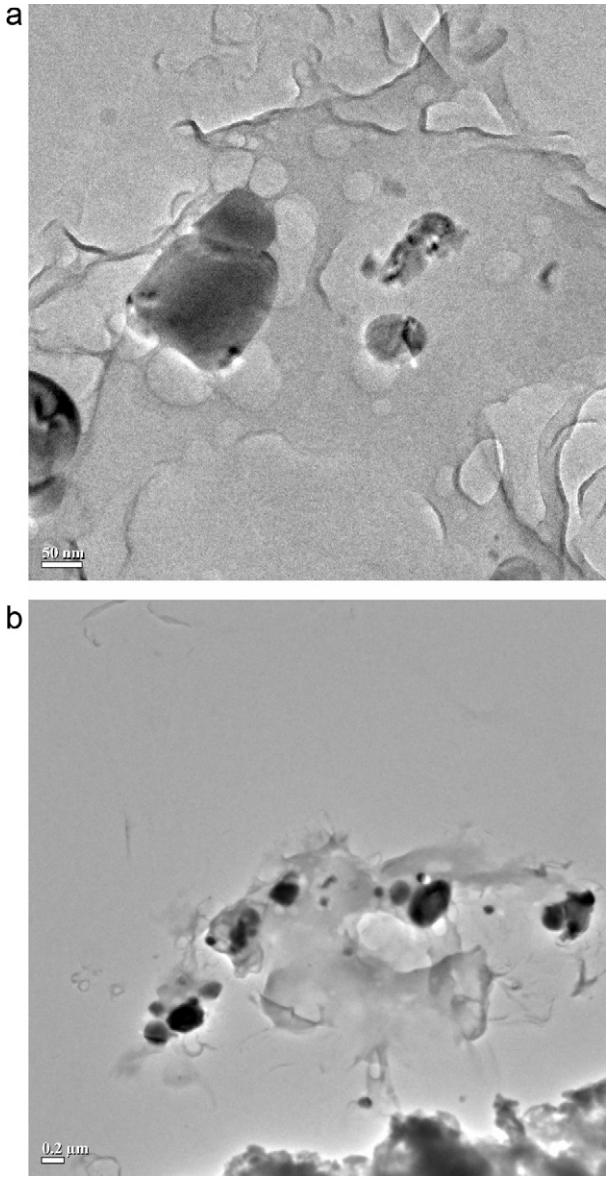

Fig. 8. TEM images of Pt/PANi composite depicting dispersion (a) and agglomeration (b).

peak corresponding to oxygen (O) highlights the following two points:

1. The porous structure of PANi facilitates water adsorption.
2. The doping of PANi by H^+ ions from weakly ionized water holds the –OH ions as counter ions for charge balance.

This particular property doubles the functionality of PANi as the material with balanced hydrophilic characteristics also. As the aromatic ring backbone of PANi is well known for its hydrophobicity, its use in PEM fuel cell [40] is well suited to enhance performance.

Table 1 compares the platinum loading on the reference MEA and the sample MEA prepared and used in this study. It could be observed that the total loading of platinum is less in the sample MEA. With 1.32% of platinum in PANi as revealed by EDX, 0.42 mg cm^{-2} of the Pt/PANi used in the sample MEA, added 5 μg cm^{-2} of platinum to the interlayer. Compared to the total loading of 0.800 mg cm^{-2} of the Pt in the reference MEA, the sample MEA has a total loading of 0.675 mg cm^{-2} of Pt and has a reduction in Pt by 18.5%.

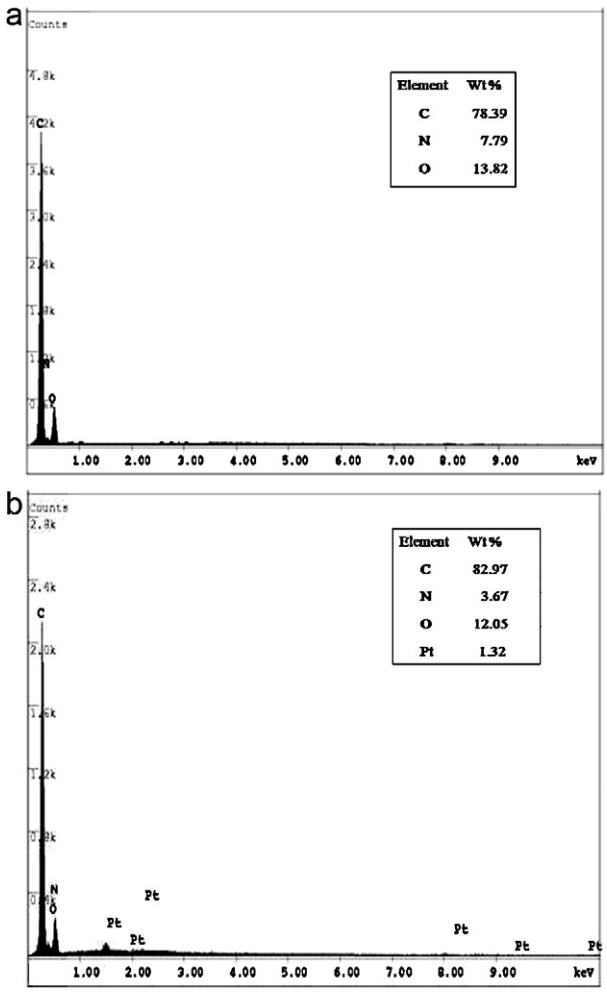

Fig. 9. (a) EDX spectrum of PANi. (b) EDX spectrum of Pt/PANi composite.

Infrared (IR) spectra of PANi and Pt/PANi are shown in Fig. 10. The IR spectra for conducting polymers give information on the vibrational excitations of the materials and also the free carrier absorption and excitation, exciton transitions or light scattering by electron [41]. The assignment of the peaks of the IR spectra is given in Table 2. Due to the method of reduction of platinum(IV) ion on the PANi matrix, PANi may also get reduced affecting its conductivity. However protonation of PANi in fuel cell occurs spontaneously by the H^+ ions from the anode reaction. The incorporation of platinum in the PANi matrix could change the corresponding vibrational frequency of the polymer. Charge transfer interactions between polymer chains and Pt nanoparticles have also been suggested [3]. Presence of water either as adsorbed species or held by ionic charge of the polymer matrix could also be observed from the IR spectra. The vibrational frequencies at 786 cm^{-1}, 2150 cm^{-1} and 3437 cm^{-1} denote the stretching, bending and combination of both of them respectively of water molecule. While a general shift in all the vibrational frequencies have been observed by the inclusion of

Table 1
Comparison of platinum loading in the reference MEA and the sample MEA prepared.

MEA	Pt loading (mg cm^{-2})			
	Anode	Cathode	GDL	Total
Reference	0.30	0.50	–	0.800
Sample	0.23	0.44	0.005	0.675

Table 2
Assignment of the infrared bands for PANi and Pt/PANi.

Band (cm^{-1})		Assignment
PANI	Pt/PANI	
786	795	Aromatic C—H bending of the aniline ring [41]
1114	1113	N=Q=N/in-plane deformation of (C—H), Q=NH^+—B [42,43]
1275 υ(C—$N^{\bullet+}$) in the polaron lattice of PANi [44]	1288 υ(C—N) of secondary aromatic amine [45,46]	Aromatic C—N stretching of the aniline unit
1468	1472	C=C stretching of aromatic ring [42,47]
2150	2167	Water (bending vibration)
2682	2631	O—H stretching
	3109	Aromatic C—H stretch
3437	3410	Adsorbed water symmetric stretching, bending [48]
3958	3869	Aromatic C—H stretching [42,43,47]

Q: Quinonoid ring; B: Benzenoid ring.

platinum, the changes of much importance for this study are the following:

1. The stretching frequency, υ(C—$N^{\bullet+}$) in the polaron lattice of PANi at 1275 cm^{-1} is altered to the stretching frequency, υ(C—N) of secondary aromatic amine in PANi, indicating a decrease in the number of polarons in Pt/PANi thereby affecting the conductivity of the Pt/PANi.
2. The combined symmetric stretching and bending frequencies of adsorbed water at 3437 cm^{-1} in PANi, decreases in strength on inclusion of Pt. The extent of the presence of adsorbed water is reduced by the presence of metallic platinum which could influence the hydrogen bonding between free water and the polymer matrix and hence facilitate water drain.

The conductivity of PANi, calculated from the resistivity measured by the four-probe method was found to be 1.055 mho cm^{-1}, while that of Pt/PANi composite was measured to be 0.764 mho cm^{-1}. The decrease in the conductivity of Pt/PANi is attributed to the decrease in the number of polarons due to the reduction of Pt(IV) on the PANi matrix which affects the oxidation state of PANi and hence its conductivity. The decrease in the number of polarons is also indicated by the IR spectra. This is not a concern for the use of Pt/PANi in the cathode interlayer as the H^+ furnished by weakly ionized water molecule and those which reach from the anode side will restore the optimum conductivity of PANi in the operating conditions of PEMFC.

The cyclic voltammograms (CV) of PANi and Pt/PANi, recorded in 0.1 M H_2SO_4 solution are shown in Fig. 11. In order to simulate the conditions of the operating fuel cell, we used a larger area of the working electrode (0.6132 cm^2) compared with the usual CV electrode, and observed a current density much higher than that of platinum electrode used in the usual CV studies. A small bump corresponding to the hydrogen reduction was observed at about −0.2 V vs Ag/AgCl in the case of PANi (Fig. 11a and b). CV patterns of Pt/PANi show oxygen reduction shoulder at about 0.6–0.7 V. In all the four cases (Fig. 11a–d) the reversible adsorption and desorption of the respective gases (N_2 and O_2) could be observed in the low current regions. These CV curves (Fig. 11) show that PANi and Pt/PANi can be used as the electrode material in PEMFC without involving any additional electrochemical reactions of their own. While the PANi electrode showed varying capacitative current on adsorption of nitrogen and oxygen, Pt/PANi registered almost similar CVs (Fig. 11c and d) highlighting its usefulness as the electrode material for electrochemical reactions. Also, the sensitivity of Pt/PANi (in terms of current density) is high when compared to that of PANi only. Both PANi and Pt/PANi showed electrostatic capacitance with the polymer as the micro electrodes and the gas (O_2) as the dielectric. This is in tune with the effective-medium-type dielectric function expected for a granular metallic system [49]. The capacitive behaviour indicates the double-layer formation at the interface [50]. This capacitance can facilitate the electrochemical reaction on the catalyst layer with ease, as a part of the activation energy is gained in the interlayer itself. The schematic diagram of the activation energy of the fuel cell in the presence of Pt/PANi interlayer can be illustrated as in Fig. 12. The double layer capacitance enhances the energy of the oxidant by 'a' as shown in Fig. 12, and hence the electrochemical reaction has a lesser energy requirement (=b − a).

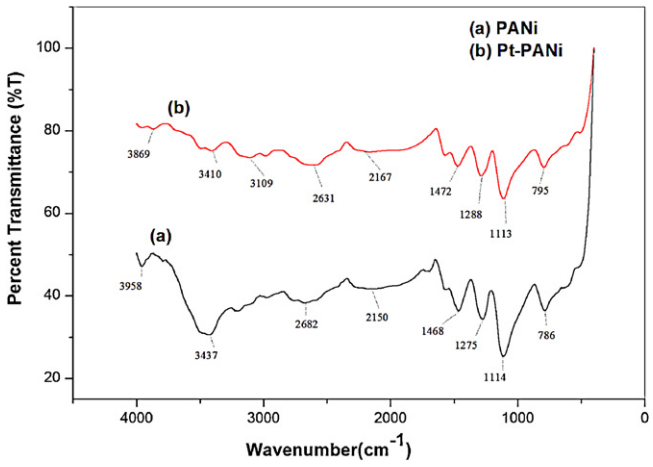

Fig. 10. Infrared spectra of (a) PANi (b) Pt–PANi.

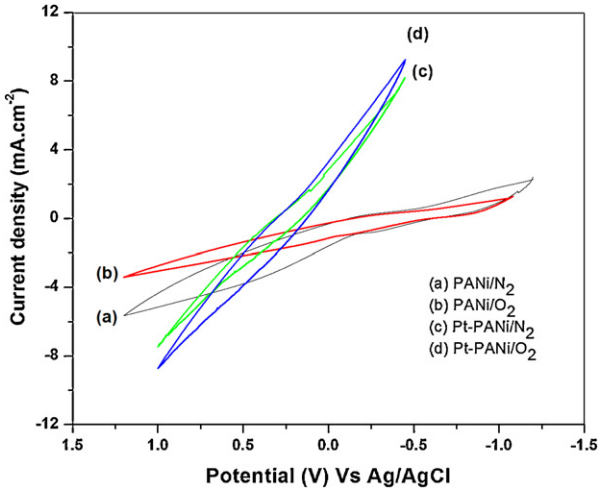

Fig. 11. Cyclic voltammograms of PANi and Pt–PANi in 0.1 M H_2SO_4: (a) PANi/N_2, (b) PANi/O_2, (c) Pt–PANi/N_2 and (d) Pt–PANi/O_2.

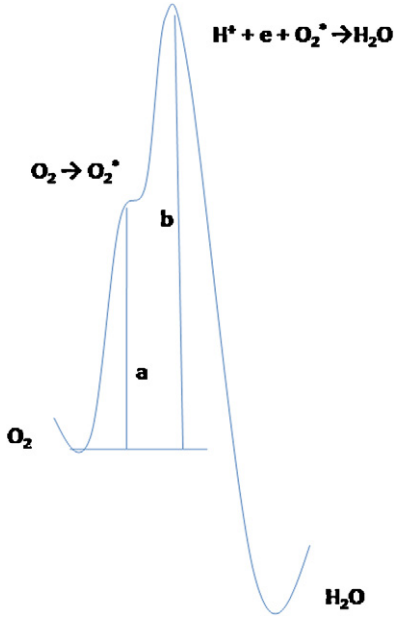

Fig. 12. Activation barrier reduction in the presence of Pt–PANi interlayer.

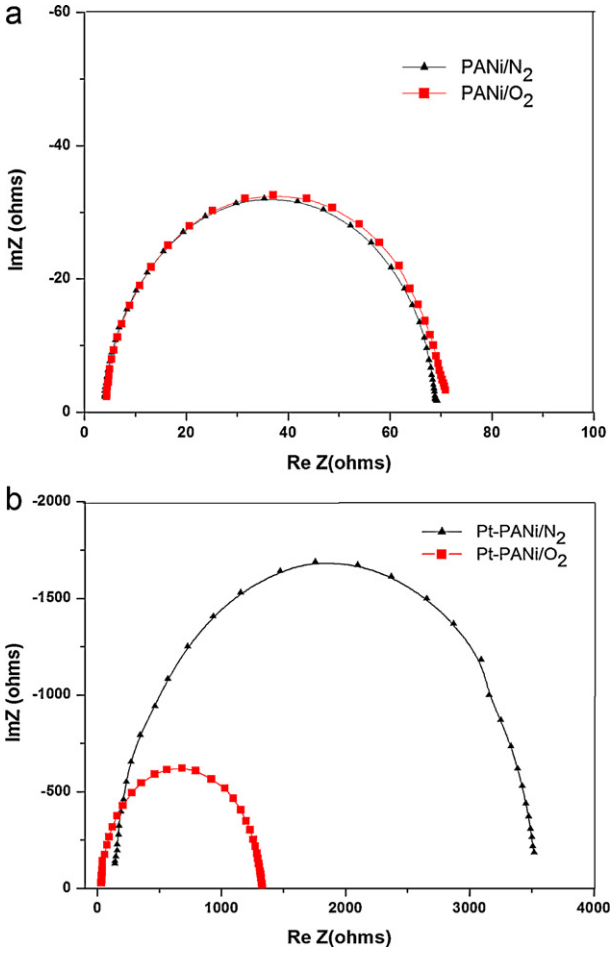

Fig. 13. (a) Nyquist plot of PANi in 0.1 M H_2SO_4 with N_2 and O_2 gases. (b) Nyquist plot of Pt–PANi in 0.1 M H_2SO_4 with N_2 and O_2 gases.

Table 3
Nyquist plot parameters of PANi and Pt–PANi.

System	R_{ct} (Ω)	C_{dl} (μF)
PANi/N_2	70	4.57
PANi/O_2	72	4.44
Pt–PANi/N_2	3500	0.09
Pt–PANi/O_2	1300	0.44

Fig. 13a and b illustrate the AC impedance spectra in 0.1 M H_2SO_4 of PANi and Pt/PANi, respectively. A semi-circle in the impedance spectrum shows a particular process, the high frequency arc corresponds to charge-transfer process and the low frequency arc denotes the diffusion process [51]. As the charge transfer occurs between the electrode and the electrolyte, the equivalent circuit of the electrochemical system contains the double-layer capacitance (C_{dl}) and charge transfer resistance (R_{ct}) in parallel for the kinetic controlled reaction. The diameter of the semi-circle in the Nyquist plot gives the value of R_{ct}. Left to right portion of the semi-circle denotes the high to low angular frequency. At the peak of the semi-circle, the angular frequency (ω) is related to C_{dl} as below, from which the C_{dl} value is determined.

$$\omega = \frac{1}{R_{ct} \cdot C_{dt}}$$

The high frequency resistance or ohmic resistance (R_s) is invariant for the PANi electrode both in N_2 and O_2 atmosphere (Fig. 13a). Ohmic resistance arises from bulk resistance and from contact resistance. The semicircle, known as the kinetic loop, is due to the interfacial kinetics of reactions and the loop decreases with increased rapidity of the electrochemical kinetics [52,53]. The charge transfer resistance (R_{ct}) and the double layer capacitance (C_{dl}) of PANi in oxygen and nitrogen atmosphere are evaluated and tabulated (Table 3). R_{ct} values for PANi are found to be almost the same in both the atmosphere and same is the case with C_{dl} also. Nitrogen is an inert gas while oxygen can undergo electrochemical reduction. But both of them are showing identical behaviour on PANi electrode. This implies that without any characteristic electrochemical changes, PANi provides an excellent support matrix for the electroactive catalysts. In the case Pt/PANi (Fig. 13b), the intrinsic surface anisotropy [54] due to the presence of Pt appears to affect the contact resistance as revealed by increased ohmic resistance. R_{ct} in nitrogen atmosphere is higher (3500 Ω) than that in oxygen atmosphere (1300 Ω), implying that adsorption of nitrogen occurs and as it does not show any electrochemical reaction, multilayer adsorption imparts high charge transfer resistance and in turn results in low C_{dl} values. Though similar multilayer adsorption can be expected in the case of oxygen also, its low R_{ct} value indicates the electroactivity of the Pt/PANi composite in the presence of O_2 avoiding multilayer build-up and thereby allowing direct electron transfer between the monolayer and the conductive medium [55]. As the GDL interlayer contains only 1% (0.005 mg cm^{-2}) of Pt compared with the loading on the cathode, it does not allow the complete electrochemical reaction to take place at the interphase itself, but reduces the activation barrier for the subsequent electrochemical reaction on the cathode side. The high R_{ct} values on the Pt/PANi could be ascribed to the combination of sluggish O_2 reduction and the limited amount of Pt in the interlayer.

The fuel cell performance of Pt/PANi coated GDL is studied at different temperatures (Fig. 14a) and also compared with that of the reference MEA that did not contain Pt/PANi interlayer (Fig. 14b and c). Fig. 14a shows the performance of fuel cell with Pt/PANi coated GDL at 60, 70 and 80 °C. The increase in performance with increase in temperature is as expected and it is due to the kinetically favoured oxygen reduction, increase in ionic conductivity and better management of the product water. Fig. 14b and c show the

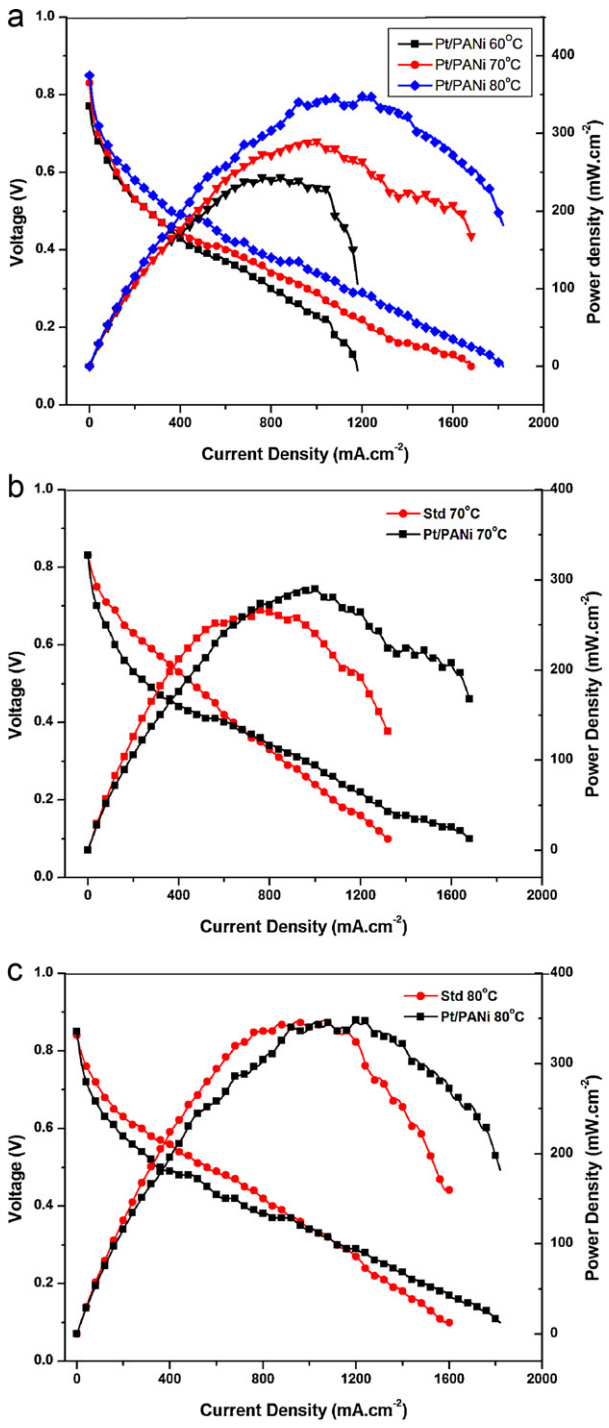

Fig. 14. (a) Fuel cell performance of Pt–PANi coated GDL using H_2/O_2 at various temperatures. (b) Fuel cell performance with and without Pt–PANi coated GDL using H_2/O_2 at 70 °C. (c) Fuel cell performance with and without Pt–PANi coated GDL using H_2/O_2 at 80 °C.

performance of the cell with Pt/PANi thin layer coated GDL and that with the standard MEA at 70 °C and 80 °C, respectively. It could be observed that Pt/PANi layer improved the performance especially at high current density values even though the overall platinum content of the Pt/PANi based MEA is lesser than that of the reference. The performance of the Pt/PANi coated GDL at 70 °C (Fig. 14b) falls behind that of the reference MEA at low current densities. Similar trend is observed at 80 °C also (Fig. 14c), but with lesser deviation in performance at low current densities compared to that at 70 °C. This is due to the fact that at low current densities, the polarization losses are mainly due to the oxygen reduction reaction which is kinetically sluggish and the losses decrease when the current is increased [23] and also due to water management issues at low current densities. In addition, the lesser amount of Pt in the Pt/PANi coated GDL could have been insufficient to pull up the sluggish kinetics in the low current density region (<600 mA cm^{-2}). Nevertheless it widens the useful current density ranges beyond that by the reference MEA with high Pt loading. Therefore it would be useful in systems requiring momentary and continuous high current densities such as in automotive applications. The same trend of widening the useful current density range is observed from the performance curves at 80 °C (Fig. 14c), which also confirms the usefulness of the Pt/PANi layer on the GDL. The peak power of the reference MEA (5 cm^2) is about 1250 mW while that of Pt/PANi coated MEA of the same area (but with 18.5% less of Pt) is 1450 mW at 70 °C. Further optimization of the interphase and GDL for higher power density is in progress.

4. Conclusions

A performance boosting interphase with Pt/PANi was introduced in the electrode assembly of proton exchange membrane fuel cell and evaluated. Conducting polyaniline was used as support onto which platinum was deposited by a simple wet chemistry method. The microporous structure of PANi facilitated not only the large useful surface area of the platinum but also its dispersion on PANi by the charge interaction. The thin layer of Pt/PANi on GDL improves the cell performance at high current densities in spite of lesser loading which is attributed to the increased capacitative current of Pt/PANi layer in the presence of O_2 thereby improving the kinetics of subsequent reduction of O_2. Chemical stability of PANi is proved by its performance at 80 °C and its electrochemical stability is proved by the featureless CV plots. Continuous matrix of PANi with large flow channels could provide an ideal surface for the three-phase equilibrium between catalyst, fuel and oxidant gases, and product water. The increase in performance is attributed to the increased capacitative current of Pt/PANi layer in the presence of O_2 thereby improving the kinetics of subsequent reduction of O_2.

Acknowledgements

NITT, India, is thankfully acknowledged for the financial assistance to LC to establish the Fuel Cell Lab. UGC, India, is acknowledged for the research facilities created through the project no. F.30-64/2004(SR).

References

[1] J. Larminie, A. Dick, Fuel Cell Systems Explained, John Wiley and Sons Ltd., UK, 2003.
[2] R.A. Fisher, Precursor Chemistry of Advanced Materials: CVD, ALD and Nanoparticles, Springer, Germany, 2005.
[3] E.A. Stefanescu, C. Darangaand, C. Stefanescu, Insight into the broad field of polymer nanocomposites: from carbon nanotubes to clay nanoplatelets, via metal nanoparticles, Materials 2 (2009) 2095–2153.
[4] J. Huang, Syntheses and applications of conducting polymer polyaniline nanofibers, Pure and Applied Chemistry 78 (1) (2006) 15–27.
[5] P.R. Hota, R.K. Parida, S.C. Das, XRD and thermal characteristic studies of conducting polymers, Journal of Reinforced Plastics and Composites 28 (2009) 265–278.
[6] D.N. Muraviev, P. Ruiz, M. Muñoz, J. Macanás, Novel strategies for preparation and characterization of functional polymer–metal nanocomposites for electrochemical applications, Pure and Applied Chemistry 80 (11) (2008) 2425–2437.
[7] J.F. Lin, V. Kamavaram, A.M. Kannan, Synthesis and characterization of CNT supported platinum nanocatalyst for PEMFCs, Journal of Power Sources 195 (2010) 466–470.

[8] D.J. Guo, H.L. Li, High dispersion and electrocatalytic properties of Pt nanoparticles on SWNT bundles, Journal of Electroanalytical Chemistry 573 (1) (2004) 197–202.
[9] P. Goriseka, V. Francetic, C.L. Lengauer, J. Macek, The reduction of hexachloroplatinic(IV) acid on the surface of alumina, Acta Chimica Slovenica 51 (2004) 203–211.
[10] B. Choi, H. Yoon, I. Park, J. Jang, Y. Sung, Highly dispersed Pt nanoparticles on nitrogen-doped magnetic carbon nanoparticles and their enhanced activity for methanol oxidation, Carbon 45 (2007) 2496–2501.
[11] H. Oh, H. Kim, Efficient synthesis of Pt nanoparticles supported on hydrophobic graphitized carbon nanofibers for electrocatalysts using noncovalent functionalization, Advanced Functional Materials 21 (20) (2011) 3954–3960.
[12] F.N. Crespilho, F. Huguenin, V. Zucolotto, P. Olivi, F.C. Nart, O.N. Oliveira Jr., Dendrimers as nanoreactors to produce platinum nanoparticles embedded in layer-by-layer films for methanol-tolerant cathodes, Electrochemistry Communications 8 (2) (2006) 348–352.
[13] A. Mani, K. Athinarayanasamy, P. Kamaraj, S. Tamil Selvan, S. Ravichandran, K.L.N. Phani, S. Pitchumani, Crystalline order in polyaniline, Journal of Materials Science Letters 14 (1995) 1594–1596.
[14] A. Nyczyk, M. Hasik, W. Turek, A. Sniechota, Nanocomposites of polyaniline, its derivatives and platinum prepared using aqueous Pt sol, Synthetic Metals 159 (2009) 561–567.
[15] G. Zotti, B. Vercelli, A. Berlin, Gold nanoparticle linking to polypyrrole and polythiophene: monolayers and multilayers, Chemistry of Materials 20 (2008) 6509–6516.
[16] F.J. Liu, L.M. Huang, T.C. Wen, A. Gopalan, Large-area network of polyaniline nanowires supported platinum nanocatalysts for methanol oxidation, Synthetic Metals 157 (2007) 651–658.
[17] S. Palmero, A. Colina, E. Muñoz, A. Heras, V. Ruiz, J. López-Palacios, Layer-by-layer electrosynthesis of Pt–polyaniline nanocomposites for the catalytic oxidation of methanol, Electrochemistry Communications 11 (2009) 122–125.
[18] I.Y. Sapurina, M.E. Kompan, A.G. Zabrodskii, J. Stejskal, M. Trchova, Nanocomposites with mixed electronic and protonic conduction for electrocatalysis, Russian Journal of Electrochemistry 43 (2007) 528–536.
[19] D. Gavre, G. Mihailescu, O. Raita, E. Indrea, S. Pruneanu, J. Rahmer, L.V. Giurgiu, Conduction electron spin resonance of Pt-nanoparticles in porous Al_2O_3 membranes, Journal of Optoelectronics and Advanced Materials 5 (1) (2003) 347–350.
[20] M. Yang, Y. Yang, Y. Liu, G. Shen, R. Yu, Platinum nanoparticles-doped sol–gel/carbon nanotubes composite electrochemical sensors and biosensors, Biosensors and Bioelectronics 21 (2006) 1125–1131.
[21] J. Solla-Gullon, A. Rodes, V. Montiel, A. Aldaz, J. Clavilier, Electrochemical characterisation of platinum–palladium nanoparticles prepared in a water-in-oil microemulsion, Journal of Electroanalytical Chemistry 554–555 (2003) 273–284.
[22] Z. Liu, M. Shamsuzzoha, E.T. Ada, W.M. Reichert, D.E. Nikles, Synthesis and activation of Pt nanoparticles with controlled size for fuel cell electrocatalysts, Journal of Power Sources 164 (2) (2007) 472–480.
[23] J. Park, M. Atobe, T. Fuchigami, Sonochemical synthesis of conducting polymer–metal nanoparticles nanocomposite, Electrochimica Acta 51 (5) (2005) 849–854.
[24] M. Wang, K.D. Woo, D.K. Kim, Preparation of Pt nanoparticles on carbon nanotubes by hydrothermal method, Energy Conversion and Management 47 (18–19) (2006) 3235–3240.
[25] J.H. Wee, K.Y. Lee, S.H. Kim, Fabrication methods for low-Pt-loading electrocatalysts in proton exchange membrane fuel cell systems, Journal of Power Sources 165 (2) (2007) 667–677.
[26] Z. Hamoudi, M.A.E. Khakani, M. Mohamedi, Binderless nanothin catalyst layers for next generation of micro-fuel cells: concept, fabrication, results and prospective, Journal of the Electrochemical Society 159 (3) (2012) B331–B339.
[27] A. Tabet-Aoul, M. Mohamedi, 3D hierarchical cauliflower-like carbon nanotubes/platinum–tin nanostructure and its electrocatalytic activity for ethanol oxidation, Journal of Materials Chemistry 22 (2012) 2491–2497.
[28] H. Wang, X. Sun, Y. Ye, S. Qiu, Radiation induced synthesis of Pt nanoparticles supported on carbon nanotubes, Journal of Power Sources 161 (2) (2006) 839–842.
[29] B. Beribey, B. Corbacioglu, Z. Altin, Synthesis of platinum particles from H_2PtCl_6 with hydrazine as reducing agent, G.U. Journal of Science 22 (4) (2009) 351–357.
[30] G. Koo, M.S. Lee, J.H. Shim, J.H. Ahn, W.M. Lee, Platinum nanoparticles prepared by a plasma-chemical reduction method, Journal of Materials Chemistry 15 (2005) 4125–4128.
[31] B.S. Rao, B.R. Kumar, V.R. Reddy, T.S. Rao, G.V. Chalapathi, Structural characterization of nickel doped cadmium sulfide, Chalcogenide Letters 8 (2) (2011) 53–58.
[32] T. Herricks, J. Chen, Y. Xia, Polyol synthesis of platinum nanoparticles: control of morphology with sodium nitrate, Nano Letters 4 (12) (2004) 2367–2371.
[33] G.S. Devi, V.J. Rao, Room temperature synthesis of colloidal platinum nanoparticles, Indian Academy of Sciences: Bulletin of Materials Science 23 (6) (2000) 467–470.
[34] A. Kumar, H.M. Joshi, A.B. Mandale, R. Srivastava, S.D. Adyanthaya, R. Pasricha, M. Sastry, Phase transfer of platinum nanoparticles from aqueous to organic solutions using fatty amine molecules, Journal of Chemical Science 116 (5) (2004) 293–300.
[35] S.C. Raghavendra, S. Khasim, M. Revanasiddhappa, M.V.N.A. Prasad, A.B. Kulkarni, Synthesis, characterization and low frequency a.c. conduction of polyaniline/fly ash composites, Bulletin of Material Science 26 (7) (2003) 733–739.
[36] S.G. Pawar, S.L. Patil, M.A. Chougule, B.T. Raut, D.M. Jundale, V.B. Patil, Polyaniline:TiO_2 nanocomposites: synthesis and characterization, Archives of Applied Science Research 2 (2) (2010) 194–201.
[37] J.G. Deng, X.B. Ding, Y.X. Pengi, A.S.C. Chan, Hybrid composite of polyaniline containing carbon nanotube, Chinese Chemical Letters 12 (11) (2001) 1037–1040.
[38] M. Wan, M. Li, J. Li, Z. Liu, Structure and electrical properties of the oriented polyaniline films, Journal of Applied Polymer Science 53 (2) (1994) 131–139.
[39] F. Şen, G. Gokagac, Different sized Platinum nanoparticles supported on carbon: an XPS study on these methanol oxidation catalysts, J. Phys. Chem. C 111 (15) (2007) 5715–5720.
[40] L. Cindrella, A.M. Kannan, Membrane electrode assembly with doped polyaniline interlayer for PEMFCs under low RH conditions, Journal of Power Sources 193 (2009) 447–453.
[41] M. Trchova, J. Stejskal, Polyaniline: the infrared spectroscopy of conducting polymer nanotubes, Pure and Applied Chemistry 83 (10) (2011) 1803–1817.
[42] G. Socrates, Infrared and Raman Characteristic Group Frequencies, John Wiley, New York, 2001.
[43] D.L. Vien, N.B. Colthup, W.G. Fateley, J.G. Grasselli, The Handbook of Infrared and Raman Characteristic frequencies of Organic Molecules, Academic Press, San Diego, 1991.
[44] M.L. Boyer, S. Quillard, G. Louarn, G. Froyer, S. Lefrant, Vibrational study of the $FeCl_3$-doped dimer of polyaniline; a good model compound of emeraldine salt, Journal of Physical Chemistry B 104 (2000) 8952–8961.
[45] E.T. Kang, K.G. Neoh, K.L. Tan, Polyaniline: a polymer with many interesting intrinsic redox states, Progress in Polymer Science 23 (1998) 277–324.
[46] M.L. Boyer, S. Quillard, E. Rebourt, G. Louarn, J.P. Buisson, A. Monkman, S. Lefrant, Vibrational analysis of polyaniline: a model compound approach, Journal of Physical Chemistry B 102 (1998) 7382–7392.
[47] L.J. Bellamy, The Infra-red Spectra of Complex Molecules, Richard Clay, Bungay, Suffolk, 1962.
[48] Y. Bouteiller, J.P. Perchard, The vibrational spectrum of $(H_2O)_2$: comparison between anharmonic ab initio calculations and neon matrix infrared data between 9000 and 90 cm^{-1}, Chemical Physics 305 (2004) 1–12.
[49] H. Kuzmany, N.S. Sariciftci, H. Neugebauer, A. Neckel, Evidence for two separate doping mechanisms in the polyaniline system, Physical Review Letters 60 (1988) 212–215.
[50] G.P. Pandey, Y. Kumar, S.A. Hashmi, Ionic liquid incorporated polymer electrolytes for super capacitor application, Indian Journal of Chemistry 49A (2010) 743–751.
[51] A. Lasia, Electrochemical impedance spectroscopy and its applications, in: B.E. Conway, J. Bockris, R.E. White (Eds.), Modern Aspects of Electrochemistry, Kluwer Academic/Plenum Publishers, New York, 1999, pp. 143–248.
[52] X. Yuan, H. Wang, J.C. Sun, J. Zhang, AC impedance technique in PEM fuel cell diagnosis—a review, International Journal of Hydrogen Energy 32 (2007) 4365–4380.
[53] P.G. Stampino, L. Omati, G. Dotelli, Electrical performance of PEM fuel cells with different gas diffusion layers, Journal of Fuel Cell Science and Technology 8 (2011) 041005–41011.
[54] G. Dotelli, L. Omati, P.G. Stampino, P. Grassini, D. Brivio, Investigation of gas diffusion layer compression by electrochemical impedance spectroscopy on running polymer electrolyte membrane fuel cells, Journal of Power Sources 196 (2011) 8955–8966.
[55] G.F. Khan, H. Shinohara, Y. Ikariyama, M. Aizawa, Electrochemical behavior of monolayer quinoprotein adsorbed on the electrode surface, Journal of Electroanalytical Chemistry and Interfacial Electrochemistry 315 (1991) 263–273.